Dications of Bis-triarylamino-[2.2]paracyclophanes: Evaluation of Excited State Couplings by GMH Analysis

Stephan Amthor and Christoph Lambert*

Institut für Organische Chemie, Universität Würzburg, Am Hubland, D-97074 Würzburg, Germany

Received: September 9, 2005; In Final Form: January 16, 2006

In this paper, we present the absorption properties of a series of bis-triarylamino-[2.2]paracyclophane diradical dications. The localized $\pi-\pi^*$ and the charge-transfer (CT) transitions of these dications are explained and analyzed by an exciton coupling model that also considers the photophysical properties of the "monomeric" triarylamine radical cations. Together with AM1-CISD-calculated transition moments, experimental transition moments and transition energies of the bis-triarylamine dications were used to calculate electronic couplings by a generalized Mulliken-Hush (GMH) approach. These couplings are a measure for interactions of the excited mixed-valence CT states. The modification of the diabatic states reveals similarities of the GMH three-level model and the exciton coupling model. Comparison of the two models shows that the transition moment between the excited mixed-valence states μ_{ab} of the dimer equals the dipole moment difference $\Delta\mu_{ag}^{(m)}$ of the ground and the excited bridge state of the corresponding monomer.

Introduction

The linear optical properties of bis-triarylamine dications are presented in this article. The understanding of the physical and chemical properties of triarylamines and their oxidized counterparts are of fundamental interest because they were widely used as hole conducting materials in organic light emitting devices,[1−10] polymer batteries,[11,12] photorefractive materials for optical data storage,[13] and in electrochromic polymers,[14] e.g., for anti-glare electrochromic mirrors as well as in the Xerox process[3,6,10,15] of laser printers and photocopiers. Bis-triarylamines with two nitrogen N redox centers that are connected by varying bridging units B are well known, and the corresponding monocationic mixed valence (MV) species $[N-B-N]^+$ are of great importance for studying hole transfer (HT) processes from one redox center to the other redox center.[16−43] A profound influence of the bridge on the HT properties has been demonstrated for several examples.[21,22,26,31,35,36] In addition to the triarylamine to triarylamine HT in MV species, it has been shown that for some systems an additional HT to the bridge B has to be taken into account for a more detailed description of the MV system.[26,36] In this context, bridge-localized MV species with excited-state mixed-valence character were described and analyzed.[26,36,44] A dihydrazine diradical dication with excited MV states was described by a similar model.[45] Apart from MV compounds, it was quite recently demonstrated that triarylamines can be used to investigate HT processes along redox cascades because the redox potential of the triarylamine redox centers can easily be tuned.[46]

Although MV species $[N-B-N]^+$ are now reasonably well understood, detailed studies of the optical properties of neutral bis-triarylamines [N−B−N] are still quite rare.[47−54] In two previous articles, the linear and nonlinear optical properties of some bis-triarylamines with varying bridging moieties, including compounds **4** and **6** presented here (Chart 1), were investigated and analyzed by a three-level model.[54,55] In this paper, the linear optical properties of bis-triarylamine dications $[N-B-N]^{2+}$ $\mathbf{1}^{2+}$, $\mathbf{4}^{2+}$, $\mathbf{6}^{2+}$, and $\mathbf{9}^{2+}$ are presented and analyzed by an exciton coupling model. The results are compared to the photophysical properties of the "monomeric" triarylamine radical cations $\mathbf{2}^{\bullet+}$, $\mathbf{3}^{\bullet+}$, $\mathbf{7}^{\bullet+}$, and $\mathbf{8}^{\bullet+}$.

In $\mathbf{1}^{2+}$, $\mathbf{4}^{2+}$, $\mathbf{5}^{2+}$, and $\mathbf{9}^{2+}$, the [2.2]paracyclophane moiety was used to bring two chromophores in close contact. This moiety provides no direct π-conjugation but allows through-space ($\pi-\pi$) and through-bond (σ) interactions.[56] It was already demonstrated by Bazan et al. that these interactions are responsible for significant $\pi-$electron delocalization between aromatic polymer chains[57−59] as well as between donor and acceptor groups.[60−65] The [2.2]paracyclophane systems, therefore, might serve as model compounds to study interchromophore interactions between two π-conjugated strands as they might occur in π-conjugated oligomers or polymers.[66,67]

The replacement of the [2.2]paracyclophane moiety in $\mathbf{4}^{2+}$ by a *p*-xylene unit in $\mathbf{6}^{2+}$ allows for the comparison of through-space and through-bond interactions with direct π-conjugation. Different arrangements of the two triarylamine chormophores as in the isomers $\mathbf{4}^{2+}$ (*pseudo-para*) and $\mathbf{5}^{2+}$ (*pseudo-ortho*) and their influence on exciton coupling will be investigated. Furthermore, a comparison of $\mathbf{1}^{2+}$, $\mathbf{4}^{2+}$, and $\mathbf{9}^{2+}$ will provide insight into the influence of the distance between the two N redox centers on the spectral features of bis-triarylamine dications with a [2.2]paracyclophane bridge.

We will compare the experimental spectral characteristics with AM1-CISD computations. These computational results will complement the observed experimental data to analyze the above-mentioned dications by a generalized Mulliken-Hush (GMH)[68−70] model to yield couplings V_{23}(GMH), which are a measure for electronic interactions of the MV excited states.

Results and Discussion

Experimental UV/Vis/NIR Spectra. The absorption spectra of all cations and dications were obtained by chemical oxidation of the neutral precursors in CH_2Cl_2 and MeCN, respectively.

* To whom correspondence should be addressed. E-mail: lambert@chemie.uni-wuerzburg.de.

10.1021/jp055098o CCC: $33.50
Published on Web 02/22/2006

CHART 1

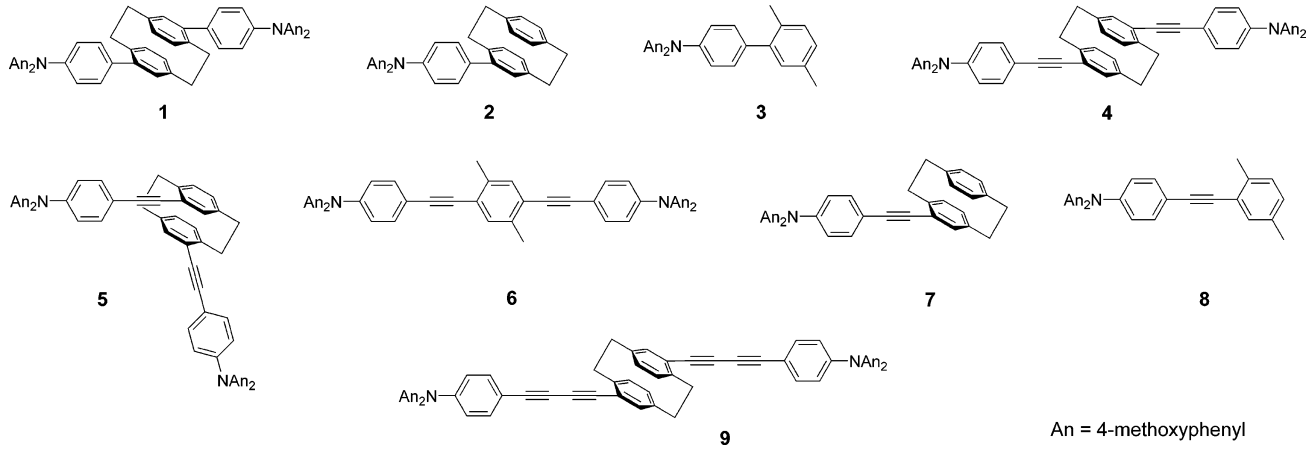

TABLE 1: Experimental Absorption Energies and Extinction Coefficients Between Parentheses in M^{-1} cm^{-1}

	$\tilde{\nu}_{NIR}/cm^{-1}$	$\tilde{\nu}_{vis}/cm^{-1}$
$\mathbf{1}^{2+}$	11300 sh (22000)	13090 (55600), 22800 sh (18000), 25900 (34800)
$\mathbf{2}^{\bullet+}$	11500 sh (10500)	13400 (24700), 23600 sh (8400), 26740 (16100)
$\mathbf{3}^{\bullet+}$		13260 (36200), 15500 sh (8600), 26180 (17400), 27600 sh (15800)
$\mathbf{4}^{2+}$	10900 (33300)	13300 (54800), 20750 (26900)
$\mathbf{5}^{2+}$	11260 (23300)	13260 (44900), 20750 (19000)
$\mathbf{6}^{2+}$	10870 (32000)	13160 (54100), 20830 (22100), 23580 (21700)
$\mathbf{7}^{\bullet+}$	10680 (15400)	13440 (23900), 20660 (12500)
$\mathbf{8}^{\bullet+}$	11500 sh (14900)	13050 (25600), 21700 sh (11900), 23150 (13500)
$\mathbf{9}^{2+}$	11100 sh (26300)	13000 (57800), 19760 (21500), 21650 (25300), 24390 (31100)

The diradical dications of bis-triarylamine compounds **1**, **4**, **5**, **6**, and **9** and the monoradical cations of **2**, **3**, **7**, and **8** show a rather intense absorption band at 13 000−13 440 cm^{-1} in CH_2Cl_2 (Figure 1 and Table 1). This band is not solvent dependent and is due to a $\pi-\pi^*$ excitation localized within the triarylamine radical cation moiety.[71] This intense triarylamine radical cation $\pi-\pi^*$ excitation is accompanied by a second, less intense absorption reflected by a distinct shoulder or even by a separated band ($\mathbf{4}^{2+}$, $\mathbf{5}^{2+}$, $\mathbf{7}^{\bullet+}$). This weaker absorption is at lower energies than the intense main signal for all compounds except $\mathbf{3}^{\bullet+}$, for which a shoulder at the higher energy side of the $\pi-\pi^*$ excitation band is observed.

As can be seen from Figure 2, there is only little influence of the solvent polarity (MeCN vs CH_2Cl_2) on the position of the intense $\pi-\pi^*$ band. However, the second, weaker band shows a distinct blue-shift, which suggests a certain CT (charge transfer) character. We suppose that the small blue-shift of the intense main peak of $\mathbf{1}^{2+}$ in MeCN relative to the peak in CH_2Cl_2 results from the strong overlap with the CT band.

Athough for biaryls $\mathbf{1}^{2+}$ and $\mathbf{2}^{\bullet+}$ with the same cyclophane "bridge" the CT band causes a shoulder at similar energy, this band is significantly blue-shifted in $\mathbf{3}^{\bullet+}$ by about 4000 cm^{-1} in CH_2Cl_2. This shift is due to the weaker electron-donor character of the *p*-xylene group compared to that of the [2.2]paracyclophane group. Comparison of the spectra of $\mathbf{4}^{2+}$, $\mathbf{6}^{2+}$, and $\mathbf{7}^{\bullet+}$ shows that the CT signal of these acetylenes is well separated from the triarylamine radical cation $\pi-\pi^*$ band and appears at similar absorption energies for all three cations. In contrast, the CT signal of the pseudo-ortho paracyclophane $\mathbf{5}^{2+}$ and the *p*-xylene derivative $\mathbf{8}^{\bullet+}$ is little blue-shifted compared to those of the CT bands of $\mathbf{4}^{2+}$, $\mathbf{6}^{2+}$, and $\mathbf{7}^{\bullet+}$. The observation of this shift of the CT absorption of *p*-xylene $\mathbf{8}^{\bullet+}$ versus cyclophanes $\mathbf{7}^{\bullet+}$ and $\mathbf{4}^{2+}$ is in accordance with the findings for $\mathbf{1}^{2+}$, $\mathbf{2}^{\bullet+}$, and $\mathbf{3}^{\bullet+}$. This is also due to the weaker electron-donor character of the *p*-xylene group compared to that of the [2.2]paracyclophane group. The $\pi-\pi^*$ and CT absorption signals of the mono-triarylamine cations $\mathbf{2}^{\bullet+}$, $\mathbf{3}^{\bullet+}$, $\mathbf{7}^{\bullet+}$, and $\mathbf{8}^{\bullet+}$ show approximately half the intensity of the absorption bands of the bis-triarylamine diradical dications $\mathbf{1}^{2+}$, $\mathbf{4}^{2+}$, $\mathbf{5}^{2+}$, $\mathbf{6}^{2+}$, and $\mathbf{9}^{2+}$. Because the oxidized triarylamine unit is predominantly responsible for the absorption properties, a doubling of the absorption intensities is expected for the symmetrical dications compared to their "monomeric" counterparts.

Exciton Coupling Model. The absorption signals of the mono-triarylamine radical cations in the vis/NIR region can be interpreted in terms of a transition polarized along the molecular principal axis *z* (connecting the nitrogen and the center of the bridge) and a transition polarized along the *x* axis (connecting the two oxygen atoms of the dianisylamine moiety; see Figure 3).

The transition polarized along *z* has a distinct CT character because positive charge can be transferred from the triarylamine to the bridge. The transition which is *x* polarized has vanishing CT character because the charge is localized at the dianisylamino groups. Thus, the intense signals at ca. 13 000 cm^{-1} can be interpreted as *x*-polarized transitions which are described as localized $\pi-\pi^*$ transitions.[71] The solvent-dependent, second, weaker absorption is attributed to the transition polarized along *z*, termed hereafter bridge CT band (CT_{bridge}). Surprisingly, the bis-triarylamine dications reveal a negative solvatochromism although the dipole moment of the ground and the Franck-Condon excited state is expected to be zero for symmetry reasons. We explain this behavior by the following model: According to Marcus-Hush theory,[72,73] the adiabatic potential energy surfaces of the ground and the two excited CT states are described by the following 3 × 3 secular determinant (eq 1), which couples three diabatic (model) states (diagonal elements) by the off-diagonal elements (electronic couplings).

$$\begin{vmatrix} \lambda\Delta^2 - E & 0 & 0 \\ 0 & \lambda\left(-\frac{1}{2}-\Delta\right)^2 + \Delta G^\circ - E & V_{23} \\ 0 & V_{23} & \lambda\left(\frac{1}{2}-\Delta\right)^2 + \Delta G^\circ - E \end{vmatrix} = 0 \quad (1)$$

Within this model, the diabatic potentials are specified as parabolic functions depending on the asymmetric electron-

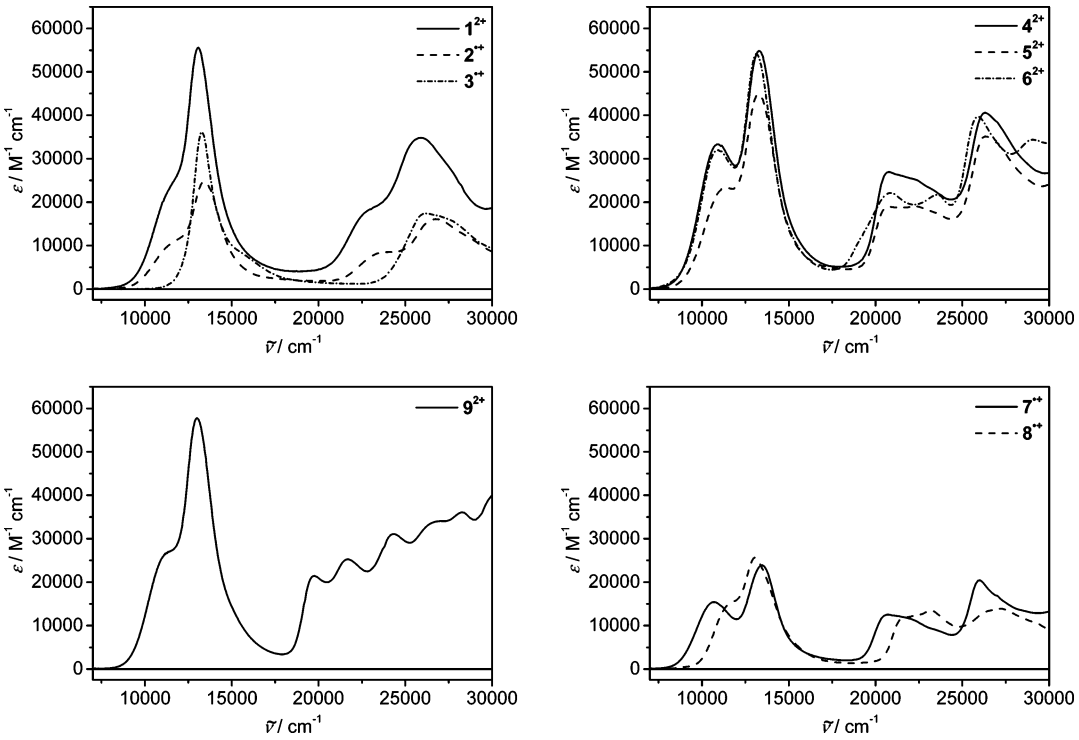

Figure 1. UV/vis/NIR spectra of radical cations and diradical dications in CH_2Cl_2.

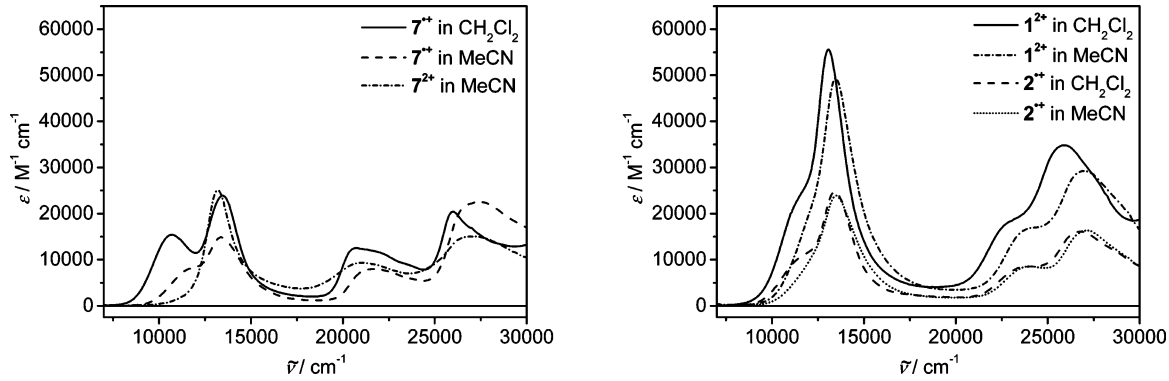

Figure 2. UV/vis/NIR spectra of $\mathbf{1}^{2+}$, $\mathbf{2}^{\bullet+}$, and $\mathbf{7}^{\bullet+}$ recorded in CH_2Cl_2 in comparison to spectra recorded in MeCN and spectrum of $\mathbf{7}^{2+}$ in MeCN.

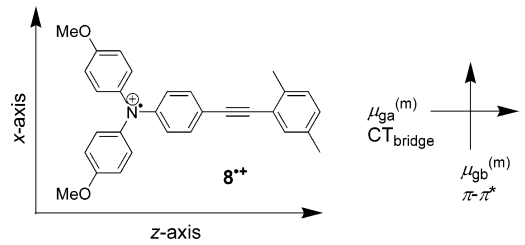

Figure 3. Transition moments of monomer $\mathbf{8}^{\bullet+}$.

transfer coordinate Δ with the minimum of the ground state located at $\Delta = 0$ and the minima of the degenerate excited states at $\Delta = -0.5$ and $\Delta = 0.5$. In principle, a symmetric coordinate would also be required for a reasonable description of the potential energy surfaces,[26,36,74] but because we lack of the necessary experimental or computational information, we restrict ourselves here to the most simple one-dimensional model. The two degenerate excited states are shifted in energy by $\Delta G°$ versus the ground state. The electronic couplings, which are a measure for the interactions between the diabatic ground and the two excited states, are neglected for simplicity ($V = 0$), and only the interactions between the excited MV states V_{23} are taken into account. Because the diabatic excited states of the "dimers" $\mathbf{1}^{2+}$, $\mathbf{4}^{2+}$, $\mathbf{5}^{2+}$, $\mathbf{6}^{2+}$, and $\mathbf{9}^{2+}$ have MV character, an increase of the solvent polarity leads to an increase of the solvent reorganization energy and, consequently, to an increase of the transition energy. i.e., to a blue-shift, as shown in Figure 4.[75] The negative solvatochromism of $\mathbf{2}^{\bullet+}$, $\mathbf{3}^{\bullet+}$, $\mathbf{7}^{\bullet+}$, and $\mathbf{8}^{\bullet+}$ can be explained analogously.

For the interpretation of the linear optical properties of the bis-triarylamines, a simple exciton coupling model[76−80] can be used. Two "monomeric" subunits, e.g., $\mathbf{8}^{\bullet+}$, with the *z*-polarized CT_{bridge} state (a) and the *x*-polarized $\pi-\pi^*$ state (b) are combined with an 180° angle to yield the C_i symmetric pseudo-para isomer $\mathbf{4}^{2+}$ and, with an 60° angle, to form the C_2 symmetric pseudo-ortho isomer $\mathbf{5}^{2+}$ (Figure 5).

Within the point-dipole approximation, exciton coupling theory yields eq 2 for the coupling integral *V*. This model uses the transition moments $\mu_{ga}^{(m1)}$ and $\mu_{ga}^{(m2)}$ from the ground state (g) to the CT_{bridge} state (a) of the two monomeric subunits (m1) and (m2), the distance $r_{m1,m2}$ of the centers of the two point-dipole transition moment vectors in the dimer, the angle between

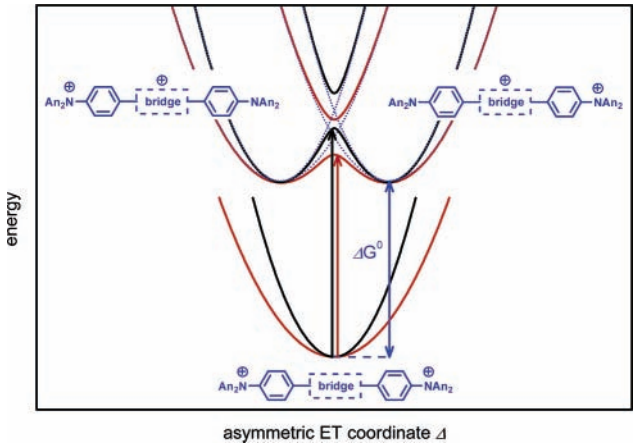

Figure 4. Adiabatic (solid) and diabatic (blue and dotted) potential energy surfaces of the "dimeric" dications with differing reorganization energies (red: small, e.g., CH_2Cl_2; black: large for MeCN). One fixed set of parameters V_{23} and $\Delta G°$ was used to calculate the potential energy surfaces.

the two transition moment vectors α_{ga}, and the two angles $\theta_{ga}^{(m1)}$ and $\theta_{ga}^{(m2)}$ between each transition moment vector and $r_{m1,m2}$ (see Table 2).

$$V = \frac{\mu_{ga}^{(m1)} \cdot \mu_{ga}^{(m2)}}{r_{m1,m2}^{3}} (\cos \alpha_{ga} - 3 \cos \theta_{ga}^{(m1)} \cdot \cos \theta_{ga}^{(m1)}) \quad (2)$$

Coupling of two monomer excited states (a) results in two excited states (a) and (b) (see Figure 5) of the dimer with a splitting energy of 2 *V*. Thus, if ground state interactions are neglected, the coupling can in principle be obtained directly from the absorption spectra because *V* equals the difference of the transition energies of the monomer and the dimer.[81] We used the trigonometric correlation of eq 2 as an estimate for the relative couplings in Figure 5. We refrain from the explicit calculation of couplings *V* by eq 2 because $r_{m1,m2}$ has a great influence on the calculated result but it cannot be determined exactly. The transition moments of the ground-state excitation of the dimer $\mu_{ga}^{(dimer)}$ to the first excited state (a) and $\mu_{gb}^{(dimer)}$ to the second excited state (b) can be calculated from the transition

TABLE 2: Estimation of Angles α and *θ*

	$\theta_{ga}^{(m1)}$	$\theta_{ga}^{(m2)}$	α_{ga}	$\theta_{gb}^{(m1)}$	$\theta_{gb}^{(m2)}$	α_{gb}
$\mathbf{1}^{2+}$						
$\mathbf{4}^{2+}$	0°	180°	180°	90°	270°	180°
$\mathbf{6}^{2+}$						
$\mathbf{5}^{2+}$	60°	120°	60°	150°	30°	120°

moment of the monomers $\mu_{ga}^{(m1)}$ or $\mu_{ga}^{(m2)}$ by the following eq 3 and eq 4.[82]

$$\mu_{ga}^{(dimer)} = \sqrt{2}\mu_{ga}^{(m1)} \cos \theta^{(m1)} = \sqrt{2}\mu_{ga}^{(m2)} \cos \theta^{(m2)} \quad (3)$$

$$\mu_{gb}^{(dimer)} = \sqrt{2}\mu_{ga}^{(m1)} \sin \theta^{(m1)} = \sqrt{2}\mu_{ga}^{(m2)} \sin \theta^{(m2)} \quad (4)$$

These two relations can also be applied to calculate the transition moments $\mu_{gc}^{(dimer)}$ and $\mu_{gd}^{(dimer)}$ of the higher-lying two excited states of the dimer (c) (compare eq 3) and (d) (compare eq 4) starting from the transition moment of the second excited state (b) of the monomers $\mu_{gb}^{(m1)}$ or $\mu_{gb}^{(m2)}$.

For C_i symmetric dications such as $\mathbf{4}^{2+}$, the linear combination of the *z*-polarized transition moments $\mu_{ga}^{(m1)}$ and $\mu_{ga}^{(m2)}$ of $\mathbf{8}^{\bullet+}$ results in only one allowed transition to state (a) of the dimer with a transition moment $\mu_{ga}^{(dimer)} = \sqrt{2}\,\mu_{ga}^{(m1)}$ derived by eq 3 (see also Figure 5). According to eq 4, the transition moment $\mu_{gb}^{(dimer)}$ of the second excited state (b) of the dimer vanishes, and thus, the second excitation is forbidden. The coupling of the $\pi-\pi^*$ states (b) of two monomeric subunits with $\mu_{gb}^{(m1)}$ and $\mu_{gb}^{(m2)}$ again results in one allowed transition to state (d) of the dimer with $\mu_{gd}^{(dimer)} = \sqrt{2}\,\mu_{gb}^{(m1)}$ and one forbidden transition to state (c) of the dimer because the transition moment $\mu_{gc}^{(dimer)}$ also vanishes. Thus, for the linear dications, the exciton coupling model predicts two allowed transitions, one to the stabilized excited CT_{bridge} state (a) (polarized along the N−N axis) and a second to the destabilized excited $\pi-\pi^*$ state (d) (polarized along the O−O axis of the dianisylamine moieties). Both states (a) and (d) have A_u symmetry. The two transitions to the excited states (c) and (b) with A_g symmetry are forbidden. Consequently, a red-shift of the CT_{bridge} excitation and a small blue-shift of the localized $\pi-\pi^*$ transition is predicted by the model.[81] The latter shift is smaller because of the weaker coupling of the

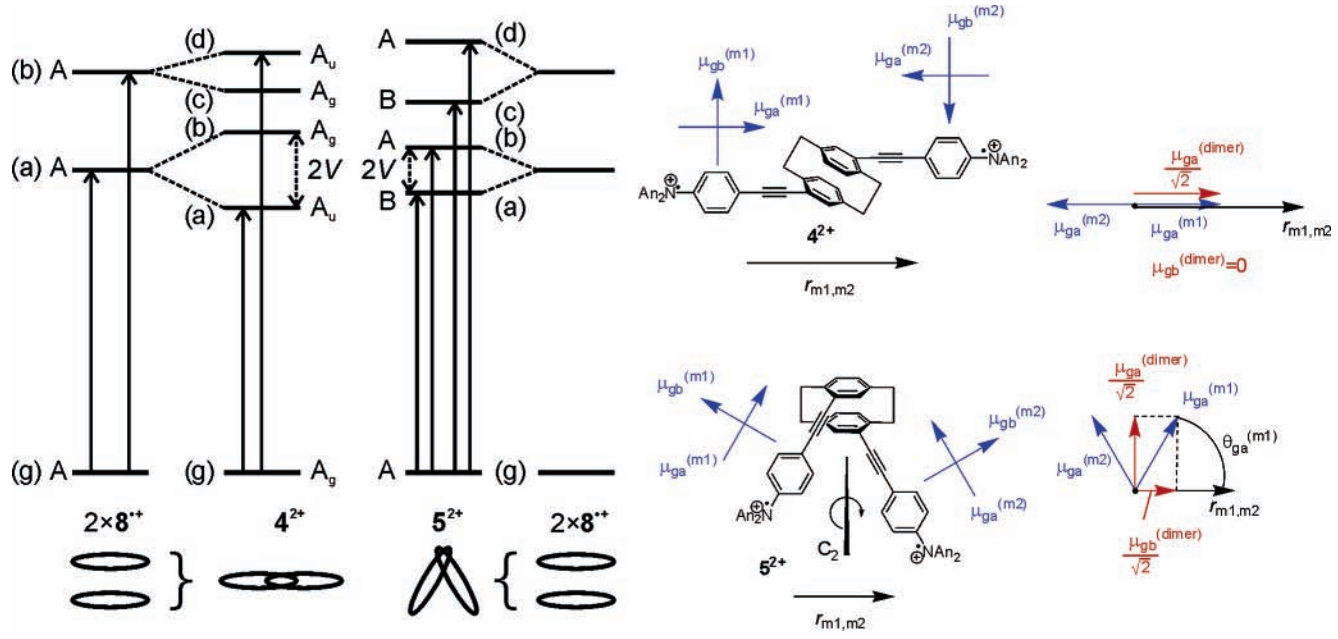

Figure 5. Exciton energy diagrams and transition moments (geometric interpretation of eqs 3 and 4) for molecular dimers $\mathbf{4}^{2+}$ and $\mathbf{5}^{2+}$.

TABLE 3: AM1-CISD Computed Absorption Energies and Transition Moments[a]

	c.i. open	state (see Figure 5)	sym.	$\tilde{\nu}$/cm^{-1}	$\tilde{\nu}_{exp}$/cm^{-1}	μ_{exp}/D	μ/D	assignment
$\mathbf{1}^{2+}$	(11,7)	a	A_u	20160	11300	5.6	7.6	CT_{bridge}
	(2,2)	b	A_g	20400	–	–	–	CT_{bridge}
		c	A_g	14020	–	–	–	$\pi-\pi^*$
		d	A_u	14100	13090	7.8	11.8	$\pi-\pi^*$
$\mathbf{2}^{\bullet+}$	(8,5)	a	A	14390	11500	4.1	6.7	CT_{bridge}
	–	b	A	15740	13400	5.1	7.7	$\pi-\pi^*$
$\mathbf{3}^{\bullet+}$	(8,5)	a	A	14590	15500	3.4	7.4	CT_{bridge}
	–	b	A	14460	13260	5.3	6.6	$\pi-\pi^*$
$\mathbf{4}^{2+}$	(11,7)	a	A_u	16100	10900	7.4	9.0	CT_{bridge}
	(2,2)	b	A_g	16190	–	–	–	CT_{bridge}
		c	A_g	14490	–	–	–	$\pi-\pi^*$
		d	A_u	14540	13300	8.4	12.7	$\pi-\pi^*$
$\mathbf{5}^{2+}$	(11,7)	a	B	15370	11260	5.9	6.5	CT_{bridge}
	(2,2)	b	A	15600			8.8	CT_{bridge}
		c	B	14620	13260	7.7	12.2	$\pi-\pi^*$
		d	A	14490			2.6	$\pi-\pi^*$
$\mathbf{6}^{2+}$	(11,7)	a	A_u	16140	10870	7.3	9.7	CT_{bridge}
	(2,2)	b	A_g	15270	–	–	–	CT_{bridge}
		c	A_g	14430	–	–	–	$\pi-\pi^*$
		d	A_u	14520	13160	7.9	12.8	$\pi-\pi^*$
$\mathbf{7}^{\bullet+}$	(8,5)	a	A	12960	10680	4.8	12.3	CT_{bridge}
	–	b	A	14970	13440	5.7	6.6	$\pi-\pi^*$
$\mathbf{8}^{\bullet+}$	(8,5)	a	A	11780	11500	3.7	10.8	CT_{bridge}
	–	b	A	15500	13050	5.8	5.9	$\pi-\pi^*$
$\mathbf{9}^{2+}$	(11,7)	a	A_u	17740	11100	6.2	7.9	CT_{bridge}
	(2,2)	b	A_g	17720	–	–	–	CT_{bridge}
		c	A_g	14360	–	–	–	$\pi-\pi^*$
		d	A_u	14390	13000	8.3	12.8	$\pi-\pi^*$

[a] Using the active orbital window with the specified MOPAC keywords "c.i." and "open".

x-polarized transition. Both predictions are fulfilled in the experimental spectra, as demonstrated by the shifts of the bridge band ($\mathbf{4}^{2+}$: -600 cm^{-1} and $\mathbf{6}^{2+}$: -630 cm^{-1}) and $\pi-\pi^*$ band ($\mathbf{4}^{2+}$: $+250$ cm^{-1} and $\mathbf{6}^{2+}$: $+110$ cm^{-1}) of $\mathbf{4}^{2+}$ and $\mathbf{6}^{2+}$ compared to the absorption signals of $\mathbf{8}^{\bullet+}$.

In principle, a similar model can be used to explain the differences in the spectra of the paracyclophane $\mathbf{1}^{2+}$ and the molecular half $\mathbf{3}^{\bullet+}$. As already mentioned, the "monomeric" fragment $\mathbf{3}^{\bullet+}$ shows a reversed order of the $\pi-\pi^*$ state (a) and the CT_{bridge} state (b) in comparison to $\mathbf{1}^{2+}$. In fact, what we obtain experimentally is a distinct red-shift of the bridge band (4200 cm^{-1}) and a small red-shift of the $\pi-\pi^*$ band (170 cm^{-1}) of the bis-triarylamine $\mathbf{1}^{2+}$compared to the molecular half $\mathbf{3}^{\bullet+}$. The shift of the bridge band is unexpectedly large, whereas the spectra of $\mathbf{1}^{2+}$ and $\mathbf{2}^{\bullet+}$ with identical bridges are very similar. We therefore suppose that $\mathbf{3}^{\bullet+}$ cannot reasonably be used as a "monomeric" subunit for the exciton coupling model. In a recent study, it was demonstrated that the sterical hindrance of ortho and meta methyl groups may have a distinct influence on the optical properties of biaryls.[83] The [2.2]paracyclophane moiety of $\mathbf{1}^{2+}$ and the *p*-xylene bridge of $\mathbf{3}^{\bullet+}$ exhibit different sterical influences and induce different torsion angles around the biaryl axes. Thus, we assume that the pronounced shift of the CT_{bridge} band of $\mathbf{3}^{\bullet+}$ versus $\mathbf{1}^{2+}$ can be traced back to the different torsional angles and, consequently, to a different extent of π-conjugation in the [2.2]paracyclophane and the *p*-xylene bridges.

The coupling of the bridge states (a) with the corresponding transition moment vectors $\mu_{ga}^{(m1)}$ and $\mu_{ga}^{(m2)}$ of two monomers $\mathbf{8}^{\bullet+}$ to the kinked C_2 symmetric dimer $\mathbf{5}^{2+}$ results according to eq 3 and eq 4 in two allowed transitions to the states (a) and (b) of the dimer (see Figure 5). The stabilized bridge state (a) of the dimer has B symmetry whereas the destabilized bridge state (b) possess A symmetry. The corresponding exciton coupling of $\pi-\pi^*$ states (3) of $\mathbf{8}^{\bullet+}$ also yields two allowed transitions to the $\pi-\pi^*$ states (c) and (d) of the dimer $\mathbf{5}^{2+}$. Here, the stabilized state (c) has B symmtery whereas the destabilized state (d) is A symmetric. The splitting energy 2 *V* of the CT_{bridge} transition is expected to be slightly smaller compared to the splitting of the CT_{bridge} state of $\mathbf{4}^{2+}$, but the splitting energy of the $\pi-\pi^*$ transition should be somewhat larger than the splitting of the $\pi-\pi^*$ states of $\mathbf{4}^{2+}$ due to the 60° orientation of the chromophores (see eq 2).[84] For symmetry reasons, the resulting transition moments of the A→A excitations are polarized along the C_2 axis, and the transition moments of A→B excitations are perpendicularly polarized to the symmetry axis. This model predicts only little influence on the transition energies but a broadening of both absorption signals in the spectrum of the V-shaped paracyclophane $\mathbf{5}^{2+}$ compared to the molecular half $\mathbf{8}^{\bullet+}$. In fact, what we obtain experimentally is a small red-shift of the CT_{bridge} band (-240 cm^{-1}) and a small blue-shift of the $\pi-\pi^*$ band ($+210$ cm^{-1}), and a broadening is not recognized.

Semiempirical Calculations. Mopac AM1-CISD calculations were performed for all radical cations and diradical dications.[85] The resulting transition energies, transition moments, and the character of the transitions are collected in Table 3.

The geometry optimizations of the monoradical cations were performed at CISD level. All dications were described as diradicals and not as the closed-shell quinoidelike systems because the optimization with solely doubly filled levels yielded somewhat larger heat of formations than the optimization as diradicals with two singly occupied levels. The computations generally yield two symmetrically allowed transitions in the vis/NIR region. One transition is polarized along the (CT_{bridge}) *z* axis and the second along the *x* axis ($\pi-\pi^*$). The calculation of the C_2 symmetric $\mathbf{5}^{2+}$ yields four allowed transitions with transition moments directed along the C_2 axis for A→A excitations and perpendicular to the C_2 axis for A→B excitations.

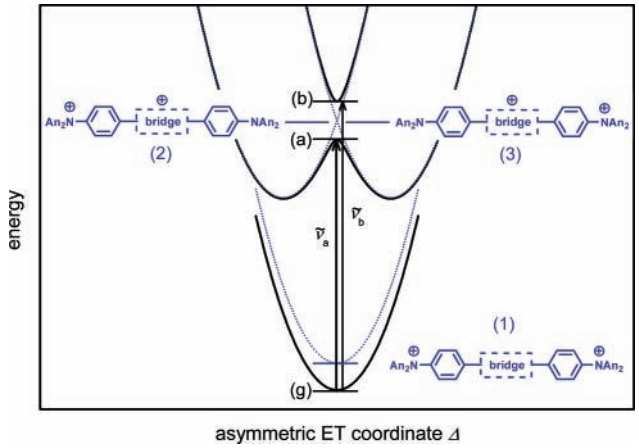

Figure 6. Adiabatic (solid) potential energy surfaces of ground state (g) and MV excited CT_{bridge} states (a) and (b) as well as diabatic (blue and dotted) potential energy surfaces (1) − (3) of bis-triarylamine diradical dications.

The energy of the localized $\pi-\pi^*$ transition of the diradical dications is generally described well, whereas the energy of the bridge band is much larger than the experimental values. The corresponding computed transition moments of the $\pi-\pi^*$ band are much larger than the experimental values. Except for that of $\mathbf{5}^{2+}$, the transition moments of the bridge band of the dications are in good agreement with the experimental values.

The calculated transition energies of the monoradical cations are generally too large compared with the experimental values. Here, the calculated transition moments of the $\pi-\pi^*$ excitation fits well with the values obtained from the experiment, but the transition moments of the bridge band are estimated too large in comparison to the experimental values.

Application of GMH Theory. The coupled CT_{bridge} states (a) (A_u or B symmetry) and (b) (A_g or A symmetry) of the bis-triaryalmine diradical dications can be conceived as excited MV states (see Figure 6).

The difference between the absorption energies of the molecular halves and the corresponding "dimers" is only a rough estimate for the coupling between the first and the second excited CT_{bridge} states. The exciton coupling model used is a simple two-state model which neglects interactions with the ground state. Therefore, we applied a GMH three-level model[86] to estimate the electronic couplings using experimental and computational data. This model was used previously to analyze a valence-delocalized bis-triarylamine radical cation MV system.[36] Here, the GMH comprises the following adiabatic (observable) states: the electronic ground state (g) and the two CT_{bridge} Franck-Condon states (a) and (b), as shown in Figure 6 (black bars).

The transition moments between the three levels (g), (a), and (b) as well as the dipole moments of these three states constitute the adiabatic transition moment matrix (eq 5). Before the elements of this matrix are explained, we mention that according to Newton et al.,[68−70] the projections of the transition moment vectors and the dipole moment vectors on an arbitrary axis have to be used for the GMH analysis. Here, we used the axis that connects the two nitrogen redox centers, and therefore, the adiabatic transition moment matrix consists of the components of the transition moment vectors as well as the components of the dipole moment vectors directed along this chosen axis. Thus, only the transition moment μ_{ga} between the ground state (g) and the first excited CT_{bridge} state (a) and the transition moment μ_{ab} between both excited CT_{bridge} states (a) and (b) differ from zero for symmetry reasons. For the C_i symmetric species, the transition moment between the ground state (g) and the second excited CT_{bridge} state (b) μ_{gb} is zero because the excitation is symmetry forbidden ($A_g \rightarrow A_g$). The transition moment vector component μ_{gb} along the N−N axis also vanishes for the C_2 symmetric molecule $\mathbf{5}^{2+}$ because A→A transitions are polarized along the C_2 axis, which is perpendicular to the N−N axis. The diagonal elements of the adiabatic transition moment matrix represent the dipole moment μ_{gg} of the ground state (g), the dipole moment μ_{aa} of state (a) and the dipole moment μ_{bb} of state (b). These moments are all zero for C_i symmetric molecules, and they are directed along the C_2 axis for a C_2 symmetric molecule, and therefore, the dipole moment projection on the N−N axis vanishes.

$$\mu_{adiab} = \begin{pmatrix} 0 & \mu_{ga} & 0 \\ \mu_{ga} & 0 & \mu_{ab} \\ 0 & \mu_{ab} & 0 \end{pmatrix} \tag{5}$$

$$\mu_{diab} = \begin{pmatrix} 0 & 0 & 0 \\ 0 & \mu_{22} & 0 \\ 0 & 0 & \mu_{33} = -\mu_{22} \end{pmatrix} \tag{6}$$

Within the GMH theory, strictly localized diabatic (model) levels 1−3 (see blue bars and structures in Figure 6) are defined with the consequence that all off-diagonal elements of the diabatic transition moment matrix $\mu_{\mathbf{diab}}$ (eq 6) become zero.[68−70] The GMH theory uses a unitary transformation of the adiabatic transition moment matrix into the corresponding diabatic matrix according to $\mu_{diab} = \mathbf{C}^t \mu_{adiab} \mathbf{C}$. This diagonalization is done by applying the matrix $\mathbf{C}$, which consists of the normalized eigenvectors of $\mu_{\mathbf{adiab}}$. The same unitary transformation with identical matrix $\mathbf{C}$ is then applied to the adiabatic energy matrix $\mathbf{H}_{diab} = \mathbf{C}^t \mathbf{H}_{adiab} \mathbf{C}$. This adiabatic energy matrix (eq 7) consists of adiabatic energy differences between the ground and the first excited state $\tilde{\nu}_a$ as well as the ground and the second excited state $\tilde{\nu}_b$. If the electronic couplings are small, we can approximate $\tilde{\nu}_a \approx \tilde{\nu}_b$.[86] This approximation has to be done because we can neither measure $\tilde{\nu}_b$ nor can it be computed accurately enough.

$$\mathbf{H}_{adiab} = \begin{pmatrix} 0 & 0 & 0 \\ 0 & \tilde{\nu}_a & 0 \\ 0 & 0 & \tilde{\nu}_b = \tilde{\nu}_a \end{pmatrix} \tag{7}$$

The resulting diabatic energy matrix (eq 8) includes the energies of the diabatic states 1−3 as the diagonal elements H_{11}, H_{22}, and H_{33} and, in addition, the electronic couplings V_{12}, V_{13}, and V_{23} as the off-diagonal elements. The coupling V_{23} between the degenerate states 2 and 3 is a direct measure for the electronic interaction between these two diabatic states.[87]

$$\mathbf{H}_{diab} = \begin{pmatrix} H_{11} & V_{12} & V_{13} \\ V_{12} & H_{22} & V_{23} \\ V_{13} & V_{23} & H_{33} \end{pmatrix} \tag{8}$$

We performed the GMH analysis for $\mathbf{1}^{2+}$, $\mathbf{4}^{2+}$, $\mathbf{5}^{2+}$, $\mathbf{6}^{2+}$, and $\mathbf{9}^{2+}$ using the available experimental transition energies $\tilde{\nu}_a$(exptl) and transition moments μ_{ga}(exptl) and AM1-CISD computational values for the missing data μ_{ab}(calcd) to estimate the coupling $V_{23}^{(d)}$.[88] The transition moment μ_{ga}(exptl) of $\mathbf{5}^{2+}$ was estimated as one-half of the transition moment obtained from spectrum deconvolution (see Experimental Section) because the two CT_{bridge} transitions to (a) and (b) that are expected cannot be analyzed separately due to a strong overlap of these signals.

TABLE 4: Input for GMH Analysis μ_{ga}(exptl), μ_{ab}(calcd) and $\tilde{\nu}_a$(exptl) and Resulting GMH Coupling Values V_{23} of Excited MV Compounds 1^{2+}, 4^{2+}, 5^{2+}, 6^{2+}, and 9^{2+}

	μ_{ga}(exptl)/D	$\Delta\mu_{ag}^{(ma)}$(calcd)[a]/D	$\Delta\mu_{ag}^{(mb)}$(calcd)[b]/D	μ_{ab}(calcd)/D	$\tilde{\nu}_a$(exptl)/cm^{-1}	$V_{23}^{(d)}$[c]/cm^{-1}	$V_{23}^{(m)}$[d]/cm^{-1}
$\mathbf{1}^{2+}$	5.6	10.4 ($\mathbf{3}^{\bullet+}$)	27.1 ($\mathbf{2}^{\bullet+}$)	22.2	11300	340	460
$\mathbf{4}^{2+}$	7.4	11.0 ($\mathbf{8}^{\bullet+}$)	26.5 ($\mathbf{7}^{\bullet+}$)	23.5	10900	490	790
$\mathbf{5}^{2+}$	3.0	6.5 ($\mathbf{8}^{\bullet+}$)[e]	13.3 ($\mathbf{7}^{\bullet+}$)[e]	16.1	11260	200	550
$\mathbf{6}^{2+}$	7.3	11.0 ($\mathbf{8}^{\bullet+}$)	–	16.4	10870	900	3320
$\mathbf{9}^{2+}$	6.2	21.7 ($\mathbf{11}^{\bullet+}$)	28.2 ($\mathbf{10}^{\bullet+}$)	33.1	11100	190	510

[a] *p*-Xylenes as monomers. [b] Cyclophanes as monomers. [c] Calculated with μ_{ab}(calcd). [d] Calculated from$\Delta\mu_{ag}^{(ma)}$ for $\mathbf{6}^{2+}$ and from $\Delta\mu_{ag}^{(mb)}$ for the remaining dications. [e] Projection on the N−N axis of the corresponding dimer $\mathbf{5}^{2+}$ calculated by multiplication of the dipole moment difference with cos 60° = 0.5.

The input values and the GMH results of all bis-triarylamine diradical dications are given in Table 4.

The bis-butadiyne $\mathbf{9}^{2+}$ with the longest N−N distance shows the smallest coupling $V_{23}^{(d)} = 190$ cm^{-1}, and the acetylene $\mathbf{4}^{2+}$ shows a medium coupling $V_{23}^{(d)} = 490$ cm^{-1}, whereas the conjugated *p*-xylyl derivative $\mathbf{6}^{2+}$ has the largest coupling $V_{23}^{(d)} = 900$ cm^{-1}. Thus, the GMH couplings $V_{23}^{(d)}$ of the "linear" para and pseudo-para compounds are large for small bridges and, especially, for molecules with direct π-conjugation between the redox centers ($\mathbf{6}^{2+}$). Compound $\mathbf{1}^{2+}$ is an exception from this general trend because the coupling $V_{23}^{(d)} = 340$ cm^{-1} is smaller than the coupling of acetylene $\mathbf{4}^{2+}$, although the AM1 calculated N−N distance (15.2 Å) of $\mathbf{1}^{2+}$ is significantly smaller compared to that of $\mathbf{4}^{2+}$ (20.1 Å). We suppose that this is a consequence of the steric hindrance which results in larger torsion angle around the biaryl axes (AM1 computed: 59° of $\mathbf{1}^{2+}$ and 46° of $\mathbf{3}^{\bullet+}$) and, therefore, in weaker interactions of the π−systems. The kinked pseudo-ortho isomer $\mathbf{5}^{2+}$ shows a coupling $V_{23}^{(d)} = 200$ cm^{-1}, which is much smaller in comparison to that of the linear pseudo-para isomer $\mathbf{4}^{2+}$, owing to the 60° orientation of the chromophores.

After having performed the GMH analysis of the excited MV states, we will now use a new definition of the diabatic states in the GMH to demonstrate the similarities between GMH theory and exciton coupling theory. In contrast to the assumption that the diabatic states are strictly localized, Kryachko introduced a modified GMH model that allows nonzero off-diagonal elements of the diabatic transition moment matrix.[89] Instead of diagonalizing the adiabatic matrixes to yield the diabatic matrixes, Kryachko generated the diabatic states by rotating the adiabatic states. This means that a Jacobi transformation of the adiabatic matrices yields the corresponding diabatic matrixes (see eqs 9−11).

$$\mathbf{J}_{ga} = \begin{pmatrix} \cos\alpha & \sin\alpha & 0 \\ -\sin\alpha & \cos\alpha & 0 \\ 0 & 0 & 1 \end{pmatrix} \mathbf{J}_{gb} = \begin{pmatrix} \cos\beta & 0 & \sin\beta \\ 0 & 1 & 0 \\ -\sin\beta & 0 & \cos\beta \end{pmatrix}$$

$$\mathbf{J}_{ab} = \begin{pmatrix} 1 & 0 & 0 \\ 0 & \cos\gamma & \sin\gamma \\ 0 & -\sin\gamma & \cos\gamma \end{pmatrix} \quad (9)$$

$$\mu_{diab} = \mathbf{J}_{ab}^{t}\, \mathbf{J}_{gb}^{t}\, \mathbf{J}_{ga}^{t} \mu_{adiab} \mathbf{J}_{ga} \mathbf{J}_{gb} \mathbf{J}_{ab} \quad (10)$$

$$\mathbf{H}_{diab} = \mathbf{J}_{ab}^{t}\, \mathbf{J}_{gb}^{t}\, \mathbf{J}_{ga}^{t} \mathbf{H}_{adiab} \mathbf{J}_{ga} \mathbf{J}_{gb} \mathbf{J}_{ab} \quad (11)$$

In the following, we will keep the adiabatic GMH labels rather than the labels introduced for the exciton coupling model. To find the analogies between GMH theory and exciton coupling theory, we have to remember that the exciton coupling model starts off with two monomeric subunits. The transition moments of these two subunits can be derived from the transition moment of the dimer by transposed eq 3 and eq 4. Accordingly, the transition moment of the two monomers is $\mu_{ga}^{(m)} = \mu_{ga}/\sqrt{2}$. A Jacobi transformation of the adiabatic transition moment matrix (5) by using the mixing angles $\alpha = 0$, $\beta = 0$, and $\gamma = 45°$ yields newly defined diabatic states with the corresponding transition moment matrix (12) (see Scheme 1). This matrix reveals that the this GMH model yields transition moments that have the same value as the transition moments evaluated for the exciton-coupled monomers $\mu_{ga}^{(m)}$. Thus, on one hand, matrix 12 can be conceived as the combination of the transition moments $\mu_{ga}^{(m)}$ and dipole moments μ_{ab} of two monomeric subunits of the exciton coupling model and, on the other hand, as being derived from two coupled, two-level systems.[36] An additional outcome of this modified GMH model is that the transition moment μ_{ab} connecting the two excited states (a) and (b) of the dimer equals the adiabatic dipole moment difference $\Delta\mu_{ag}^{(m)} = \mu_{aa}^{(m)} - \mu_{gg}^{(m)}$ between the ground state (g) and the CT_{bridge} excited state (a) of the *p*-xylene monomer ($\Delta\mu_{ag}^{(ma)}$) or cyclophane monomer ($\Delta\mu_{ag}^{(mb)}$). This dipole moment difference could, in principle, be determined experimentally or computationally more accurately than the transition moment μ_{ga} of the dimer.

SCHEME 1

$$\mu_{adiab} = \begin{pmatrix} 0 & \mu_{ga} & 0 \\ \mu_{ga} & 0 & \mu_{ab} \\ 0 & \mu_{ab} & 0 \end{pmatrix} \quad (5)$$

45° rotation / exciton coupling

$$\mu_{diab} = \begin{pmatrix} 0 & \frac{\mu_{ga}}{\sqrt{2}} & \frac{\mu_{ga}}{\sqrt{2}} \\ \frac{\mu_{ga}}{\sqrt{2}} & -\mu_{ab} & 0 \\ \frac{\mu_{ga}}{\sqrt{2}} & 0 & \mu_{ab} \end{pmatrix} \quad (12)$$

$$\mathbf{H}_{adiab} = \begin{pmatrix} 0 & 0 & 0 \\ 0 & \tilde{\nu}_a & 0 \\ 0 & 0 & \tilde{\nu}_b \end{pmatrix} \quad (7)$$

45° rotation / exciton coupling

$$\mathbf{H}_{diab} = \begin{pmatrix} 0 & 0 & 0 \\ 0 & \frac{\tilde{\nu}_a + \tilde{\nu}_b}{2} & \frac{\tilde{\nu}_a - \tilde{\nu}_b}{2} \\ 0 & \frac{\tilde{\nu}_a - \tilde{\nu}_b}{2} & \frac{\tilde{\nu}_a + \tilde{\nu}_b}{2} \end{pmatrix} \quad (13)$$

The 45° rotation is equivalent to a block diagonalization of matrix 5.[90] If we now apply the 45° rotation to the adiabatic energy matrix, we obtain the corresponding diabatic energy matrix (13) (Scheme 1). This matrix consists of the energies of the diabatic states as the diagonal elements and the electronic couplings as the off-diagonal elements. As shown in Scheme 1, this matrix (13) exhibits no coupling between the ground and the excited states but only a coupling between the two excited states. The energy of the diabatic states equals the midpoint between the two transition energies $\tilde{\nu}_a$ and $\tilde{\nu}_b$ of the dimer. The result of the Jacobian transformation of the adiabatic energy matrix (7) is equivalent to a two-level model where only the interactions between the two excited states are taken into account. Again, this is equivalent to the exciton coupling model where the exciton splitting energy equals twice the exciton coupling energy.

CHART 2

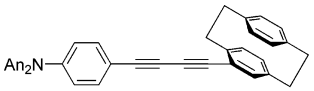

10

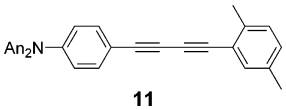

11

To prove the finding that μ_{ab} of the dimer equals the adiabatic dipole moment difference $\Delta\mu_{ag}^{(m)}$ of the monomer, we performed further AM1-CISD calculations to compare the dipole moment differences of the monomers with the calculated transition moments μ_{ab} of the corresponding dimers. The differences $\Delta\mu_{ag}^{(ma)}$ of the *p*-xylene derivatives $\mathbf{3}^{\bullet+}$, $\mathbf{8}^{\bullet+}$, and $\mathbf{11}^{\bullet+}$ as well as the differences $\Delta\mu_{ag}^{(mb)}$ of the [2.2]paracyclophanes $\mathbf{2}^{\bullet+}$, $\mathbf{7}^{\bullet+}$, and $\mathbf{10}^{\bullet+}$ are given in Table 4. The compounds $\mathbf{10}^{\bullet+}$ and $\mathbf{11}^{\bullet+}$ (see Chart 2), which have not been synthesized, are the two corresponding monomers of $\mathbf{9}^{2+}$.

For the [2.2]paracyclophanes $\mathbf{1}^{2+}$, $\mathbf{4}^{2+}$, $\mathbf{5}^{2+}$, and $\mathbf{9}^{2+}$, the calculated dipole moment difference $\Delta\mu_{ag}^{(ma)}$ of the corresponding *p*-xylene derivatives $\mathbf{3}^{\bullet+}$, $\mathbf{8}^{\bullet+}$, and $\mathbf{11}^{\bullet+}$ is significantly smaller than the transition moment μ_{ab}, whereas smaller deviations of $\Delta\mu_{ag}^{(ma)}$ and μ_{ab} are found for the *p*-xylene $\mathbf{6}^{2+}$. Because the [2.2]paracyclophane moiety is a stronger donor than the *p*-xylene moiety, all $\Delta\mu_{ag}^{(mb)}$ values are significantly larger than $\Delta\mu_{ag}^{(ma)}$. The differences $\Delta\mu_{ag}^{(mb)}$ of the [2.2]paracyclophanes $\mathbf{2}^{\bullet+}$, $\mathbf{7}^{\bullet+}$, and $\mathbf{10}^{\bullet+}$ are in good agreement with the corresponding transition moments μ_{ab} of $\mathbf{1}^{2+}$, $\mathbf{4}^{2+}$, $\mathbf{5}^{2+}$, and $\mathbf{9}^{2+}$. Thus, this comparison indicates that the [2.2]paracyclophane monomers $\mathbf{2}^{\bullet+}$, $\mathbf{7}^{\bullet+}$, and $\mathbf{10}^{\bullet+}$ are more suitable monomeric building blocks for the corresponding dications $\mathbf{1}^{2+}$, $\mathbf{4}^{2+}$, $\mathbf{5}^{2+}$, and $\mathbf{9}^{2+}$, whereas $\mathbf{6}^{2+}$ can be traced back to the *p*-xylene monomer $\mathbf{8}^{\bullet+}$.

The dipole moment differences $\Delta\mu_{ag}^{(ma)}$ and $\Delta\mu_{ag}^{(mb)}$ of the adequate monomers were used instead of μ_{ab} of the GMH analysis according to eqs 5−7. The resulting couplings $V_{23}^{(m)}$ are given in Table 4. These couplings are all larger than the couplings $V_{23}^{(d)}$, in particular for $\mathbf{6}^{2+}$ where $V_{23}^{(m)}$ is more than three times larger than $V_{23}^{(d)}$. These deviations reveal that the GMH analysis shows a pronounced dependence on the transition moment μ_{ab} or $\Delta\mu_{ag}^{(m)}$, respectively. However, the trends of $V_{23}^{(m)}$ and $V_{23}^{(d)}$ are similar with the exception that the couplings $V_{23}^{(m)}$ of $\mathbf{5}^{2+}$ and $\mathbf{9}^{2+}$ are somewhat smaller than $V_{23}^{(m)}$ of $\mathbf{1}^{2+}$.

As demonstrated above, the exciton coupling model is suitable for the interpretation of the energetic shifts of the absorption bands of $\mathbf{4}^{2+}$ and $\mathbf{6}^{2+}$ versus the corresponding absorption bands of *p*-xylene $\mathbf{8}^{\bullet+}$. But, as discussed in this section, the monomer $\mathbf{8}^{\bullet+}$ is not a good model to fulfill the relation between $\Delta\mu_{ag}^{(m)}$ of the monomer and μ_{ab} of the corresponding dimer $\mathbf{4}^{2+}$. This relation demonstrates nicely that choosing the proper monomeric model compound is crucial for a correct analysis.

Conclusions

Although the differences in the vis/NIR spectra of the [2.2]paracyclophanes $\mathbf{1}^{2+}$, $\mathbf{2}^{\bullet+}$, $\mathbf{4}^{2+}$, $\mathbf{5}^{2+}$, $\mathbf{7}^{\bullet+}$, $\mathbf{9}^{2+}$, and the *p*-xylyl $\mathbf{6}^{2+}$ are small, the spectral features of the "dimers" $\mathbf{4}^{2+}$ and $\mathbf{6}^{2+}$ can be explained by exciton coupling of two "monomers" $\mathbf{8}^{\bullet+}$.

The combination of AM1-CISD-computed transition moments connecting the two excited CT_{bridge} states μ_{ab}(calcd) with experimental transition moments μ_{ga}(exp.) and transition energies $\tilde{\nu}_a$(exptl) allows us to apply a GMH analysis. Within this GMH three-level model, the coupling $V_{23}^{(d)}$ between the first and the second excited state, which were described as mixed-valence states, were calculated. These couplings are a direct measure for the electronic interactions of the excited bridge states (a) and (b). The trends of the couplings $V_{23}^{(d)}$ are in reasonable agreement with the exciton coupling model. On one hand, this coupling decreases with increasing bridge size, as demonstrated for $\mathbf{4}^{2+}$ and $\mathbf{9}^{2+}$, and on the other hand, the coupling significantly increases when the bridge reveals direct $\pi-$conjugation, as in compound $\mathbf{6}^{2+}$. In a recent study, a similar trend was found for the complete set of the corresponding monocationic ground-state MV species $\mathbf{1}^{\bullet+}$, $\mathbf{4}^{\bullet+}$, $\mathbf{5}^{\bullet+}$, $\mathbf{6}^{\bullet+}$, and $\mathbf{9}^{\bullet+}$.[74] The 60° orientation of the chromophores in $\mathbf{5}^{2+}$ results in a distinct lowering of the coupling V_{23} in comparison to V_{23} of the pseudo-para derivative $\mathbf{4}^{2+}$. For the corresponding monocations $\mathbf{4}^{\bullet+}$ and $\mathbf{5}^{\bullet+}$, the lowering of the coupling is less pronounced. In the set of dications, $\mathbf{1}^{2+}$ is an exception because the value estimated by the GMH is smaller than that of $\mathbf{4}^{2+}$ although $\mathbf{1}^{2+}$ has the smallest bridge. We explain this discrepancy by steric hindrance, which results in larger torsion angles at the biaryl axes of $\mathbf{1}^{2+}$ (59°) and, therefore, in reduced interactions of the π-systems. This assumption also explains the unusually large experimental shift of the CT_{bridge} absorption energy $\tilde{\nu}_a$ of $\mathbf{1}^{2+}$ versus $\tilde{\nu}_a$ of its corresponding molecular half $\mathbf{3}^{\bullet+}$ (torsion angle 46°).

A modification to the diabatic states of the GMH theory was done by applying a Jacobi transformation to the adiabatic matrixes. A 45° Jacobi rotation of the adiabatic matrixes results in block diagonalized diabatic matrixes. These two matrixes (12 and 13) represent the starting point of the exciton coupling model because their matrix elements consist of values which correspond to the monomeric subunits. The exciton coupling model starts off with the monomeric subunits, whereas the GMH starts with the dimer, and thus, the modified GMH can be regarded as an inversion of exciton coupling and vice versa. An additional outcome of this modified GMH is that the transition moments μ_{ab} connecting the two excited states (a) and (b) of the dimer equals the adiabatic dipole moment difference $\Delta\mu_{ag}^{(m)} = \mu_{aa}^{(m)} - \mu_{gg}^{(m)}$ between the ground state (g) and the CT_{bridge} excited state (a) of the monomer. This dipole moment difference was determined by semiempirical AM1-CISD computations. The comparison of the transition moments μ_{ab} with the dipole moment differences of the monomers $\Delta\mu_{ag}^{(m)}$ leads to the conclusion that the adequate monomers for the [2.2]paracyclophanes $\mathbf{1}^{2+}$, $\mathbf{4}^{2+}$, $\mathbf{5}^{2+}$, and $\mathbf{9}^{2+}$ are the corresponding cyclophanes $\mathbf{2}^{\bullet+}$, $\mathbf{7}^{\bullet+}$, and $\mathbf{10}^{\bullet+}$, whereas the *p*-xylene $\mathbf{6}^{2+}$ can be related to the *p*-xylene monomer $\mathbf{8}^{\bullet+}$. Although the exciton coupling is suitable for the interpretation of the shifts, the relation between $\Delta\mu_{ag}^{(m)}$ and μ_{ab} shows the limits of the simple exciton coupling model. The dipole moment differences of the monomers $\Delta\mu_{ag}^{(m)}$ were used for the GMH analysis to calculate $V_{23}^{(m)}$. These couplings $V_{23}^{(m)}$ are somewhat larger than $V_{23}^{(d)}$, but the trends of $V_{23}^{(m)}$ and $V_{23}^{(d)}$ are similar with the exception of $V_{23}^{(m)}$ of $\mathbf{1}^{2+}$ being even smaller than $V_{23}^{(m)}$ of $\mathbf{5}^{2+}$ and $\mathbf{9}^{2+}$.

In conclusion, our study demonstrates a close similarity of the exciton and GMH models. Because exciton coupling can be viewed as a coherent energy transfer process, a close analogy of charge transfer and energy transfer processes results. Furthermore, with the exception of $\mathbf{1}^{2+}$, the couplings V_{23} of the excited MV dications $\mathbf{4}^{2+}$, $\mathbf{5}^{2+}$, $\mathbf{6}^{2+}$, and $\mathbf{9}^{2+}$ show a very

similar trend to the couplings of the corresponding monocationic ground-state MV compounds $\mathbf{4}^{\bullet+}$,$\mathbf{5}^{\bullet+}$,$\mathbf{6}^{\bullet+}$, and $\mathbf{9}^{\bullet+}$.

Experimental Section

UV/Vis/NIR Spectroscopy. The UV/vis/NIR spectra of the radical cations and dications in MeCN were obtained by stepwise addition of $10^{-2}-10^{-3}$ M $NOBF_4$/MeCN via a microliter syringe to a solution of the compounds ($3-7 \times 10^{-5}$ M). Because the oxidation process is rather slow using $NOBF_4$ in MeCN, one has to wait approximately 30 min after each addition before the spectrum could be recorded. The extinction coefficients obtained in MeCN are too small due to the slight instability of the radical cations under the conditions employed. The spectra in CH_2Cl_2 were obtained by dropwise addition of $10^{-2}-10^{-3}$ M $SbCl_5/CH_2Cl_2$ in the same way. The quick oxidation process in CH_2Cl_2 allows very short periods between the addition of the oxidation agent and spectrum measurement. The vis/NIR region of the absorption spectra recorded in CH_2Cl_2 were fitted by three Gaussian functions; whereas a single function was fitted to the CT_{bridge} band, two Gaussian functions were fitted to the $\pi-\pi^*$ absorption signal. For the radical cation $\mathbf{3}^{\bullet+}$ in CH_2Cl_2, two functions were fitted to each absorption signal. Equation 14 was used to calculate the experimental transition moments from the integrals of the reduced (divided by $\tilde{\nu}$) Gaussian functions.

$$\mu_{exp} = \sqrt{\frac{3\ h\ c\ \epsilon_0 \ln 10}{2000\ \pi^2\ N} \cdot \frac{9n}{(n^2+2)^2} \cdot \int \frac{\epsilon(\tilde{\nu})}{\tilde{\nu}} d\tilde{\nu}} \qquad (14)$$

AM1-CISD Calculations. All calculations were carried out using the AM1 parametrization implemented in the MOPAC97 program.[85] The optimization of all bis-triarylamine diradical dications $\mathbf{1}^{2+}$, $\mathbf{4}^{2+}$, $\mathbf{6}^{2+}$, and $\mathbf{9}^{2+}$ were performed with symmetry restrictions (C_2 for $\mathbf{5}^{2+}$ and C_i for the remaining) by the BFGS method. The configuration interaction included singles and doubles excitations (CISD) within an active orbital window comprising the three highest doubly occupied, the two highest singly occupied, and the two lowest unoccupied orbitals. The structures of the mono-triarylamine radical cations $\mathbf{2}^{\bullet+}$, $\mathbf{3}^{\bullet+}$, $\mathbf{7}^{\bullet+}$, $\mathbf{8}^{\bullet+}$, $\mathbf{10}^{\bullet+}$, and $\mathbf{11}^{\bullet+}$ were optimized without symmetry restrictions in Cartesian coordinates by the BFGS method. Here, the active orbital space consisted of the four highest doubly occupied, one singly occupied, and the two lowest unoccupied orbitals. The Pulay's procedure was used as the self-consistent field (SCF) converger of all calculations. To improve the calculation results, larger active orbitals windows have been used (see Table 3), and a single SCF cycle was computed. The values of c.i.(n,m) in Table 3 are specified as n the number of orbitals in the active space, m the number of doubly filled levels, and the values of the open (n_1,n_2) keyword consists of n_1 as the number of electrons in n_2 levels. The used open (2,2) keyword adds two more electrons to the two lowest unoccupied levels of the active space defined by the c.i. keyword, and thus, the doubly charged bis-triarylamines are described as diradical dications. For the single SCF cycle of the radical cation $\mathbf{10}^{\bullet+}$, a c.i. (9,6) and for $\mathbf{11}^{\bullet+}$, a c.i.(8,5) were used.

Acknowledgment. We are grateful to the Deutsche Forschungsgemeinschaft and the Volkswagenstiftung for financial support.

References and Notes

(1) Tang, C. W. *Appl. Phys. Lett.* **1986**, *48*, 183−185.
(2) Tang, C. W.; van Slyke, S. A. *Appl. Phys. Lett.* **1987**, *51*, 913−915.
(3) Borsenberger, P. M.; Weiss, D. S. *Organic Photoreceptors for Imaging Systems*; Marcel Dekker: New York, 1993.
(4) Kolb, E. S.; Gaudiana, R. A.; Mehta, P. G. *Macromolecules* **1996**, *29*, 2359−2364.
(5) Fujikawa, H.; Tokito, S.; Taga, Y. *Synth. Met.* **1997**, *91*, 161−162.
(6) Thelakkat, M.; Fink, R.; Haubner, F.; Schmidt, H.-W. *Macromol. Symp.* **1998**, *125*, 157−164.
(7) Giebeler, C.; Antoniadis, H.; Bradley, D. D. C.; Shirota, Y. *Appl. Phys. Lett.* **1998**, *72*, 2448−2450.
(8) Redecker, M.; Bradley, D. D. C.; Inbasekaran, M.; Wu, W. W.; Woo, E. P. *Adv. Mater.* **1999**, *11*, 241−246.
(9) Braig, T.; Müller, D. C.; Gross, M.; Meerholz, K.; Nuyken, O. *Macromol. Rapid Commun.* **2000**, *21*, 583−589.
(10) Thelakkat, M. *Macromol. Mater. Eng.* **2002**, *287*, 442−461.
(11) Takeuchi, M.; Kobayashi, M.; Shishikawa, R.; Sakai, T.; Nakamura, H.; Konuma, H. *Jpn. Kokai Tokkyo Koho* **1986**.
(12) Kaeriyama, K.; Suda, M.; Sato, M.; Osawa, Y.; Ishikawa, M.; Kawai, M. *Jpn. Kokai Tokkyo Koho* **1988**.
(13) Moerner, W. E.; Silence, S. M. *Chem. Rev.* **1994**, *94*, 127−155.
(14) Nishikitani, Y.; Kobayashi, M.; Uchida, S.; Kubo, T. *Electrochim. Acta* **2001**, *46*, 2035−2040.
(15) Stolka, M.; Yanus, J. F.; Pai, D. M. *J. Phys. Chem.* **1984**, *88*, 4707.
(16) Bonvoisin, J.; Launay, J.-P.; Van der Auweraer, M.; De Schryver, F. C. *J. Phys. Chem.* **1994**, *98*, 5052−5057; **Erratum: 1996**, *100* (45), 18006.
(17) Bonvoisin, J.; Launay, J.-P.; Verbouwe, W.; Van der Auweraer, M.; De Schryver, F. C. *J. Phys. Chem.* **1996**, *100*, 17079−17082.
(18) Stickley, K. R.; Blackstock, S. C. *Tetrahedron Lett.* **1995**, *36*, 1585−1588.
(19) Lambert, C.; Nöll, G. *Angew. Chem., Int. Ed.* **1998**, *37*, 2107−2110.
(20) Lambert, C.; Nöll, G.; Schmalzlin, E.; Meerholz, K.; Bräuchle, C. *Chem.−Eur. J.* **1998**, *4*, 2129−2135.
(21) Lambert, C.; Nöll, G. *J. Am. Chem. Soc.* **1999**, *121*, 8434−8442.
(22) Lambert, C.; Nöll, G.; Hampel, F. *J. Phys. Chem. A* **2001**, *105*, 7751−7758.
(23) Coropceanu, V.; Malagoli, M.; Andre, J. M.; Brédas, J.-L. *J. Chem. Phys.* **2001**, *115*, 10409−10416.
(24) Lambert, C.; Nöll, G. *Chem.−Eur. J.* **2002**, *8*, 3467−3477.
(25) Coropceanu, V.; Malagoli, M.; Andre, J. M.; Brédas, J.-L. *J. Am. Chem. Soc.* **2002**, *124*, 10519−10530.
(26) Lambert, C.; Nöll, G.; Schelter, J. *Nat. Mater.* **2002**, *1*, 69−73.
(27) Lambert, C.; Nöll, G. *J. Chem. Soc., Perkin Trans. 2* **2002**, 2039−2043.
(28) Nelsen, S. F.; Konradsson, A. E.; Weaver, M. N.; Telo, J. P. *J. Am. Chem. Soc.* **2003**, *125*, 12493−12501.
(29) Lambert, C.; Nöll, G.; Zabel, M.; Hampel, F.; Schmalzlin, E.; Bräuchle, C.; Meerholz, K. *Chem.−Eur. J.* **2003**, *9*, 4232−4239.
(30) Lambert, C. *ChemPhysChem* **2003**, *4*, 877−880.
(31) Coropceanu, V.; Lambert, C.; Nöll, G.; Brédas, J.-L. *Chem. Phys. Lett.* **2003**, *373*, 153−160.
(32) Yano, M.; Ishida, Y.; Aoyama, K.; Tatsumi, M.; Sato, K.; Shiomi, D.; Ichimura, A.; Takui, T. *Synth. Met.* **2003**, *137*, 1275−1276.
(33) Yano, M.; Aoyama, K.; Ishida, Y.; Tatsumi, M.; Sato, K.; Shiomi, D.; Takui, T. *Polyhedron* **2003**, *22*, 2003−2008.
(34) Jones, S. C.; Coropceanu, V.; Barlow, S.; Kinnibrugh, T.; Timofeeva, T.; Brédas, J. L.; Marder, S. R. *J. Am. Chem. Soc.* **2004**, *126*, 11782−11783.
(35) Coropceanu, V.; Gruhn, N. E.; Barlow, S.; Lambert, C.; Durivage, J. C.; Bill, T. G.; Nöll, G.; Marder, S. R.; Brédas, J.-L. *J. Am. Chem. Soc.* **2004**, *126*, 2727−2731.
(36) Lambert, C.; Amthor, S.; Schelter, J. *J. Phys. Chem. A* **2004**, *108*, 6474−6486.
(37) Szeghalmi, A. V.; Erdmann, M.; Engel, V.; Schmitt, M.; Amthor, S.; Kriegisch, V.; Nöll, G.; Stahl, R.; Lambert, C.; Leusser, D.; Stalke, D.; Zabel, M.; Popp, J. *J. Am. Chem. Soc.* **2004**, *126*, 7834−7845.
(38) Heckmann, A.; Lambert, C.; Goebel, M.; Wortmann, R. *Angew. Chem., Int. Ed.* **2004**, *43*, 5851−5856.
(39) Low, P. J.; Paterson, M. A. J.; Puschmann, H.; Goeta, A. E.; Howard, J. A. K.; Lambert, C.; Cherryman, J. C.; Tackley, D. R.; Leeming, S.; Brown, B. *Chem.−Eur. J.* **2004**, *10*, 83−91.
(40) Lambert, C.; Risko, C.; Coropceanu, V.; Schelter, J.; Amthor, S.; Gruhn, N. E.; Durivage, J.; Brédas, J.-L. *J. Am. Chem. Soc.* **2005**, *127*, 8508−8516.
(41) Barlow, S.; Risko, C.; Coropceanu, V.; Tucker, N. M.; Jones, S. C.; Levi, Z.; Khrustalev, V. N.; Antipin, M. Y.; Kinnibrugh, T. L.; Timofeeva, T.; Marder, S. R.; Brédas, J. L. *Chem. Commun.* **2005**, 764−766.
(42) Chiu, K. Y.; Su, T. H.; Huang, C. W.; Liou, G. S.; Cheng, S. H. *J. Electroanal. Chem.* **2005**, *578*, 283−287.

(43) Dümmler, S.; Roth, W.; Fischer, I.; Heckmann, A.; Lambert, C. *Chem. Phys. Lett.* **2005**, *408*, 264−268.
(44) Lockard, J. V.; Zink, J. I.; Trieber, D. A.; Konradsson, A. E.; Weaver, M. N.; Nelsen, S. F. *J. Phys. Chem. A* **2005**, *109*, 1205−1215.
(45) Lockard, J. V.; Zink, J. I.; Konradsson, A. E.; Weaver, M. N.; Nelsen, S. F. *J. Am. Chem. Soc.* **2003**, *125*, 13471−13480.
(46) Lambert, C.; Schelter, J.; Fiebig, T.; Mank, D.; Trifonov, A. *J. Am. Chem. Soc.* **2005**, *127*, 10600−10610.
(47) Hreha, R. D.; George, C. P.; Haldi, A.; Domercq, B.; Malagoli, M.; Barlow, S.; Brédas, J.-L.; Kippelen, B.; Marder, S. R. *Adv. Funct. Mater.* **2003**, *13*, 967−973.
(48) Albota, M.; Beljonne, D.; Brédas, J.-L.; Ehrlich, J. E.; Fu, J.-Y.; Heikal, A. A.; Hess, S. E.; Kogej, T.; Levin, M. D.; Marder, S. R.; McCord-Maughon; Dianne, P.; Joseph, W.; Rockel, H.; Rumi, M.; Subramaniam, G.; Webb, W. W.; Wu, X.-L.; Xu, C. *Science* **1998**, *281*, 1653−1656.
(49) Reinhardt, B. A.; Brott, L. L.; Clarson, S. J.; Dillard, A. G.; Bhatt, J. C.; Kannan, R.; Yuan, L. X.; He, G. S.; Prasad, P. N. *Chem. Mater.* **1998**, *10*, 1863−1874.
(50) Rumi, M.; Ehrlich, J. E.; Heikal, A. A.; Perry, J. W.; Barlow, S.; Hu, Z.; McCord-Maughon, D.; Parker, T. C.; Roeckel, H.; Thayumanavan, S.; Marder, S. R.; Beljonne, D.; Brédas, J.-L. *J. Am. Chem. Soc.* **2000**, *122*, 9500−9510.
(51) Chung, S. J.; Lin, T. C.; Kim, K. S.; He, G. S.; Swiatkiewicz, J.; Prasad, P. N.; Baker, G. A.; Bright, F. V. *Chem. Mater.* **2001**, *13*, 4071−4076.
(52) Cho, B. R.; Piao, M. J.; Son, K. H.; Lee, S. H.; Yoon, S. J.; Jeon, S. J.; Cho, M. H. *Chem.−Eur. J.* **2002**, *8*, 3907−3916.
(53) Pond, S. J. K.; Rumi, M.; Levin, M. D.; Parker, T. C.; Beljonne, D.; Day, M. W.; Brédas, J. L.; Marder, S. R.; Perry, J. W. *J. Phys. Chem. A* **2002**, *106*, 11470−11480.
(54) Strehmel, B.; Amthor, S.; Schelter, J.; Lambert, C. *ChemPhysChem* **2005**, *6*, 893−896.
(55) Amthor, S.; Dümmler, S.; Fischer, I.; Lambert, C.; Schelter, J. Excited Mixed-Valence States of Symmetrical Donor−Acceptor−Donor π-Systems. *J. Phys. Chem. A* **2006**, Accepted for publication.
(56) Heilbronner, E.; Maier, J. P. *Helv. Chim. Acta* **1974**, *57*, 151−159.
(57) Bazan, G. C.; Oldham, J., Jr.; Lachicotte, R. J.; Tretiak, S.; Chernyak, V.; Mukamel, S. *J. Am. Chem. Soc.* **1998**, *120*, 9188−9204.
(58) Verdal, N.; Godbout, J. T.; Perkins, T. L.; Bartholomew, G. P.; Bazan, G. C.; Kelley, A. M. *Chem. Phys. Lett.* **2000**, *320*, 95−103.
(59) Bartholomew, G. P.; Bazan, G. C. *Acc. Chem. Res.* **2001**, *34*, 30−39.
(60) Zyss, J.; Ledoux, I.; Volkov, S.; Chernyak, V.; Mukamel, S.; Bartholomew, G. P.; Bazan, G. C. *J. Am. Chem. Soc.* **2000**, *122*, 11956−11962.
(61) Bartholomew, G. P.; Bazan, G. C. *J. Am. Chem. Soc.* **2002**, *124*, 5183−5196.
(62) Moran, A. M.; Bartholomew, G. P.; Bazan, G. C.; Kelley, A. M. *J. Phys. Chem. A* **2002**, *106*, 4928−4937.
(63) Bartholomew, G. P.; Rumi, M.; Pond, S. J. K.; Perry, J. W.; Tretiak, S.; Bazan, G. C. *J. Am. Chem. Soc.* **2004**, *126*, 11529−11542.
(64) Hong, J. W.; Woo, H. Y.; Liu, B.; Bazan, G. C. *J. Am. Chem. Soc.* **2005**, *127*, 7435−7443.
(65) Woo, H. Y.; Hong, J. W.; Liu, B.; Mikhailovsky, A.; Korystov, D.; Bazan, G. C. *J. Am. Chem. Soc.* **2005**, *127*, 820−821.
(66) Salhi, F.; Collard, D. M. *Adv. Mater.* **2003**, *15*, 81−85.
(67) Salhi, F.; Lee, B.; Metz, C.; Bottomley, L. A.; Collard, D. M. *Org. Lett.* **2002**, *4*, 3195−3198.
(68) Creutz, C.; Newton, M. D.; Sutin, N. J. *J. Photochem. Photobiol. A* **1994**, *82*, 47−59.
(69) Cave, R. J.; Newton, M. D. *Chem. Phys. Lett.* **1996**, *249*, 15−19.
(70) Newton, M. D. *Adv. Chem. Phys.* **1999**, *106*, 303−375.
(71) Amthor, S.; Noller, B.; Lambert, C. *Chem. Phys.* **2005**, *316*, 141−152.
(72) Brunschwig, B. S.; Sutin, N. In *Electron Transfer in Chemistry*, 1 ed.; Balzani, V., Ed.; VCH: Weinheim, 2001; Vol. 2, pp 583−617.
(73) Brunschwig, B. S.; Creutz, C.; Sutin, N. *Chem. Soc. Rev.* **2002**, *31*, 168−184.
(74) Amthor, S.; Lambert, C. *J. Phys. Chem. A* **2005**, *110*, 1177−1189.
(75) In comparison to the strong influence of the solvent polarity on λ, we assume $\Delta G°$ to be only weakly affected by the solvent, and therefore, $\Delta G°$ is kept constant for the calculation of the potential surfaces in Figure 4.
(76) Kasha, M. In *Physical Processes in Radiation Biology*; Augenstein, L., Mason, R., Rosenberg, B., Eds.; Academic Press: New York, 1964.
(77) McRae, E. G.; Kasha, M. In *Physical Process in Radiation Biology*; Augenstein, L., Mason, R., Rosenberg, B., Eds.; Academic Press: New York, 1964; pp 23−42.
(78) Kasha, M.; Rawls, H. R.; El-Bayoumi, M. A. *Pure Appl. Chem.* **1965**, *11*, 371−392.
(79) Hayashi, M.; Shiu, Y. J.; Chang, C. H.; Liang, K. K.; Chang, R.; Yang, T. S.; Islampour, R.; Yu, J.; Lin, S. H. *J. Chin. Chem. Soc.* **1999**, *46*, 381−393.
(80) Beenken, W. J. D.; Dahlbom, M.; Kjellberg, P.; Pullerits, T. *J. Chem. Phys.* **2002**, *117*, 5810−5820.
(81) Interactions between the ground states that result in an energy lowering are neglected as they are supposed to be small.
(82) Kasha, M.; Rawls, H. R.; El-Bayoumi, M. A. *Pure Appl. Chem.* **1965**, *11*, 371−392. Equation 14 of this paper was corrected by us.
(83) Mank, D.; Raytchev, M.; Amthor, S.; Lambert, C.; Fiebig, T. *Chem. Phys. Lett.* **2003**, *376*, 201−206.
(84) This thesis acts on the assumption that the distances $r_{m1,m2}$ and the transition moments are similar (see eq 2).
(85) Stewart, J. J. P. *MOPAC97*; Fujitsu Limited: 1997.
(86) Newton, M. D. *Chem. Rev.* **1991**, *91*, 767−792.
(87) Although we imply the tight-binding approximation to the GMH model with the assumption that the excited states do not interact directly, the GMH analysis yields values for the coupling between these two excited CT_{bridge} states.
(88) Because the accuracy of the calculated transition moment μ_{ab} is not known, mixing experimental data and computational data to evaluate V_{23} may involve greater errors.
(89) Kryachko, E. S. *J. Phys. Chem. A* **1999**, *103*, 4368−4370.
(90) This would be more obvious if the indices 1 and 2 of the matrix elements were exchanged.